Lightweight and flexible Cu(In,Ga)Se2 solar minimodules: Toward 20% photovoltaic efficiency and beyond

Shogo Ishizuka (✉ shogo-ishizuka@aist.go.jp)

AIST

Yukiko Kamikawa

AIST

Jiro Nishinaga

AIST

Abstract

Lightweight and flexible photovoltaic solar cells and modules are promising technologies leading to wide usage of light-to-electricity energy conversion devices. This communication presents the prospects of Cu(In,Ga)Se2 (CIGS)-based lightweight and flexible photovoltaic devices. The current status of flexible CIGS minimodules with photovoltaic efficiencies greater than 18% and future directions to enhance their performance toward 20% and beyond are discussed. The effects of cell separation edges, which are formed through a mechanical, laser, or photolithography scribing process used to fabricate solar cells and modules, on the device performance are also discussed. It was found that mechanically scribed CIGS device edges, which are present in conventional solar cells and modules, cause deterioration of device performance. In other words, further improvement is expected with proper passivation/termination treatment of the edges or replacing mechanical scribing with a damage-free separation process.

Introduction

The development of lightweight and flexible photovoltaic solar cells that can be installed in places with severe weight restrictions, curved surfaces, or with difficulty of the utilization of conventional Si-based solar cells, is expected to lead to the widespread use of solar energy. Thin-film photovoltaic technologies, including Cu(In,Ga)Se$_2$ (CIGS), CdTe, and other chalcogenide and organic-inorganic hybrid perovskite solar cells, are promising for realizing this type of application, namely, highly efficient, cost-effective, and lightweight flexible photovoltaic devices[1]. Among thin-film photovoltaic technologies, CIGS-based solar cells are an attractive option owing to their advantages of relatively high energy conversion efficiency, long-term stability, relatively short energy payback time, and small carbon footprint of products[2]. To date, the photovoltaic efficiency of CIGS-based solar modules fabricated using rigid glass substrates has been approaching 20%, for instance, 19.8% (Avancis, 665.4 cm^2, 110 cells)[3,4], 19.8% (Solar Frontier, 24.2 cm^2, 12 cells)[5], and 19.2% (Solar Frontier, 841 cm^2, 70 cells)[5].

One of the notable features of CIGS-based modules is that they can be fabricated using grid electrodes and monolithically interconnected structures. Here, the grid electrode structure comprises independent cells connected with bus-bar and grid electrodes, similar to the structure of conventional Si-based solar modules, whereas the monolithically interconnected structure is fabricated with patterned cells monolithically interconnected on a single substrate (Fig. 1). The highly efficient CIGS solar modules with photovoltaic efficiencies greater than 19% demonstrated on the aforementioned glass substrates have a monolithically interconnected structure. Although both the module structures have merits and demerits, it is not a question whether they are better or not. Nonetheless, a monolithically interconnected structure has the merit of realizing thinner and lighter solar modules, owing to the absence of metal wires on the module surface. To date, photovoltaic efficiencies greater than 18% have been demonstrated for CIGS solar (mini)modules fabricated on non-glass flexible substrates, regardless of the grid electrode[6] or monolithically interconnected structure[7].

In this communication, recent developments in the photovoltaic performance of lightweight and flexible monolithically interconnected CIGS solar minimodules are presented. The remaining issues in CIGS solar cells and modules toward higher photovoltaic efficiencies are also discussed.

Results And Discussion

Lightweight and flexible monolithically interconnected CIGS solar minimodules

To obtain enhanced device performance from CIGS-based solar cells and modules, the control of alkali metal doping is essential. The effects of various alkali metals (Li, Na, K, Rb, and Cs) on CIGS thin-film and device properties have been widely studied[8–15]. The use of heavier elements such as Rb and Cs has been reported to be more effective in obtaining higher photovoltaic efficiencies[12,13]. In contrast, the aforementioned 19.8%-efficiency CIGS submodule (Avancis, 665.4 cm^2, 110 cells) was demonstrated using only a relatively light alkali-metal Na-postdeposition treatment (PDT)[4]. This report suggests that the beneficial effect of alkali metal doping depends not only on the alkali metal species but also on the doping methods and processes, including the quantity and timing of the supply of alkali metals and other experimental conditions.

The photovoltaic properties of CIGS solar minimodules #1 and #2 obtained with different alkali metal PDTs in our laboratory are summarized in Table 1. These photovoltaic parameters were obtained from independently certified measurements, which were performed at the Photovoltaic Calibration, Standards, and Measurement Team of the Renewable Energy Research Center, AIST, and the Japan Electrical Safety and Environment Technology Laboratories (JET), respectively, after heat-light soaking (HLS) treatments. Variations in parameters such as open-circuit voltage (V_{OC}), short-circuit current density (J_{SC}), and fill factor (FF) are assumed to be due to the difference in elemental composition ratio [Ga]/([Ga] + [In]) (GGI) and CdS buffer thickness of these devices instead of the different alkali metal species used for PDT (minimodule #2 has a higher GGI value and a thicker CdS layer than those of #1, see the Methods section). This result indicates that the current technique can demonstrate approximately 18.5% efficiency CIGS minimodules on flexible substrates using a monolithically interconnected structure. Figure 2a shows a photograph of the CIGS solar minimodule #1. In comparison with the weight of conventional photovoltaic solar modules in the range of 10−20 kg/m^2, the weight of our CIGS minimodules fabricated using 0.2-mm-thick flexible ceramic sheets as the substrate is equivalent to one-tenth of their weight. The beneficial effect of metastable acceptor activation with HLS or heat-bias soaking (HBS) treatments on CIGS small-area solar cells grown with alkali metal PDT has been reported in the literature[16,17]. It was found that a similar beneficial effect of enhancing photovoltaic efficiency with HLS treatments can be obtained from the CIGS minimodules, irrespective of the alkali metal species used for the PDTs, as shown in Fig. 2b. The enhancement in photovoltaic performance was due to improvements in V_{OC} and FF, and this result was similar to that for small-area cells[16,17].

For further development of CIGS photovoltaic devices, enhancement of the photovoltaic efficiencies of small-area cells, namely the baseline of device performance, is essential. In addition to alkali-metal doping, Ag- and S-alloying for modification and control of the energy band structure in CIGS devices, improvement in the bulk crystal quality, and surface and back interface (buffer/CIGS and CIGS/Mo interfaces) modification are current hot topics in the CIGS community[4,13,18–23]. These approaches are expected to lead to further enhancements in lightweight and flexible CIGS minimodule efficiencies from the current 18.5% level demonstrated with quaternary CIGS photoabsorbers in this study to 20% and beyond.

Effects of cell separation edges on photovoltaic performance

As mentioned, the suppression of carrier recombination at the interface and in the bulk of CIGS thin-film devices is important for improving the photovoltaic efficiencies. To date, much effort has been devoted to suppress recombination at the surface (buffer/CIGS) and back (CIGS/Mo) interfaces, and in the bulk of CIGS photoabsorbers, including grain boundaries and grain inside[24]. In addition to these recombination issues, it is suggested that scribed edges of CIGS photoabsorbers, namely, cross-sections of a CIGS device formed in cell and module fabrication processes, are likely to be one of the important origins leading to recombination and concomitant degradation of device performance. Nevertheless, to date, there have been few discussions on the effect of mechanically scribed edges on the photovoltaic performance. Therefore, in this section, the effect of mechanical scribing (MS), which has been used as a standard technique, on photovoltaic performance is comparatively studied with photolithographically formed edges.

MS is usually employed for P2 and P3 patterning processes for monolithically interconnected module fabrication, as shown in Fig. 1b. Laser scribing techniques have been proposed to unify P1–P3 patterning processes[25,26]. At present, however, a decreasing shunt resistance occurring at laser-scribed edges remains an issue for proper cell separation[26]. A decrease in the resistance is not a problem for P2 edges; however, it leads to significant degradation of the P3 edges owing to the incomplete separation of cell strings. The question is, then, whether MS is a perfect separation process or not, namely, whether the scribed edges are negligible as recombination centers and no photovoltaic performance degradation is expected. If not, further improvement can be expected to enhance the photovoltaic performance of CIGS cells and modules with proper passivation/termination treatments. Hence, the effect of MS on the device performance was studied using small-area cells on soda-lime glass (SLG) substrates. Note that only few institutes, such as the National Renewable Energy Laboratory, have employed a photolithography (PhL) cell separation process to date[27]; and thus, there have been few reports regarding the damage effect of conventional MS on photovoltaic performance when compared to the use of PhL.

The CIGS small-area cells fabricated using MS and PhL cell separation processes are shown in Fig. 3. Details of the CIGS device fabrication process can be found in the Methods section. Although PhL may

be a relatively high-cost and time-consuming process compared with MS, it has been used to precisely define the cell area[27]. As shown in Fig. 3, the cell edge formed with PhL is sharper and thus more precise than that formed with MS. PhL etched only the CdS and upper layers, thus the CIGS layer remained. Nonetheless, electron-beam induced current (EBIC) measurements revealed that the expansion of the space charge region in the CIGS layer was clearly halted on the edge, implying successful cell separation. This is consistent with the constant values observed for J_{SC} and external quantum efficiency (EQE), irrespective of MS or PhL, as shown in Fig. 4.

In this study, variations in the photovoltaic parameters obtained from four types of CIGS cells were examined. These are CIGS solar cells fabricated with (w/) and without (w/o) RbF-PDT using MS or PhL cell separation. No anti-reflection coating (ARC) was used, and no metastable acceptor activation treatment (such as HLS or HBS treatments) was performed before the measurements. Figure 4a shows the data obtained from the eight cells for each type

of device. A systematic variation was observed in the photovoltaic efficiencies, and the use of RbF-PDT and PhL led to an enhancement in the performance. It was found that the use of RbF-PDT was effective in enhancing V_{OC} and FF, similar to the results shown in previous reports[12,28], whereas the use of PhL was particularly effective in improving FF. No significant variation was observed in J_{SC}. The current density (J)−voltage (V) and EQE curves obtained from the best cells for each type of device are shown in Figs. 4b and 4c. The diode parameters obtained from the corresponding cells are summarized in Table 2, where R_{sh}, R_s, A, and J_0 denote the shunt resistance, series resistance, diode ideality factor, and reverse saturation current density, respectively. Variations observed in the $J−V$ and EQE curves are reasonably consistent with the variations in photovoltaic parameters, and the use of RbF-PDT enhanced V_{OC} (Fig. 4b). The use of PhL improved the leakage current, as can be seen in the third quadrant, and no significant variation in EQE was observed regardless of the cell type (Fig. 4c). Notably, the use of PhL leads to an increase in R_{sh}, resulting in an improvement in FF, and thus, photovoltaic efficiency. The light R_{sh} (R_{sh} obtained under illumination) of typical CIGS cells fabricated with MS was $700−800$ W cm^2, which was almost consistent with the values obtained in our previous report[29], In contrast, the light R_{sh} of CIGS cells fabricated with PhL was significantly high and greater than 5000 W cm^2, and the dark R_{sh} (R_{sh} obtained under dark conditions) was nominally infinite. This result indicates that conventional cell edges formed with MS cause degradation of the photovoltaic performance, and thus there is room for further improvement in the cell separation process.

Illumination intensity dependence

One of the important properties required for practical applications of photovoltaic solar cells and modules is their photovoltaic performance under low illumination conditions, irrespective of whether they are used indoor or outdoor. Thus, variations in photovoltaic performance with light intensity (irradiance dependence) were measured under simulated sunlight with neutral density (ND) filters. Figure 5a shows the $J−V$ curves and variations in solar cell parameters measured under various light intensity conditions

ranging from 1 to 0.01 sun (nominally equivalent to from 100,000 to 1000 lx). For this experiment, two small-area (0.5 cm^2) cells (red and black lines and markers) randomly selected from PhL- and MS-separated RbF-PDT CIGS devices with photovoltaic efficiencies of 20.1 and 18.6% at 1 sun, respectively, without HLS treatments, were used. It is known that the photovoltaic performance under low illumination conditions significantly depends on R_{sh}, and CIGS cells with relatively low R_{sh} show a steep drop in V_{oc} and FF under low illumination conditions[30]. This trend could be observed for the MS-processed CIGS cell shown in Fig. 5a. On the other hand, the PhL cell showed no such drastic performance degradation under low illumination conditions. On the contrary, even a slight improvement was observed for the photovoltaic efficiency. These two CIGS cells were fabricated in identical growth batches from the Mo back contact layer to ZnO:Al surface electrode layer deposition processes, thus, only the cell separation process was different. The PhL- and MS-processed CIGS cells demonstrated comparable photovoltaic efficiencies of 18.5–20% at 1 sun, but the difference between the photovoltaic performance, particularly V_{oc} and FF, and concomitant maximum output power (P_{max}) became large with decreasing light intensity. The variation trend observed for the PhL-processed CIGS cell was quite similar to the simulation results of an ideal cell with $R_s \approx 0$ and $R_{sh} \approx$ infinite[30]. This result indicates that the effect of cell separation process on photovoltaic performance, that is, the MS technique conventionally used for cell and module fabrication, is nonnegligible and a quite important issue as well as the interface and bulk issues of CIGS devices.

Figure 5b shows the lightweight and flexible CIGS minimodules (size: 8×10 and 2×10 cm^2, P1: laser scribing, P2 and P3: MS, demonstration products fabricated using relatively low photovoltaic efficiency [approximately 15% or less] minimodules) generating electricity and lighting a green LED under room light (fluorescent tubes) with approximately 200 lx (nominally equivalent to 0.002 sun) illumination, indicating that CIGS solar modules can be useful light-harvesting devices even under low illumination conditions such as on the floor in the office of the author. Note that these CIGS solar minimodules were fabricated using conventional MS for the P3 patterning process, and thus, further improvements are expected with modifying the P3 patterning.

The lightweight and flexible CIGS minimodules with photovoltaic efficiencies greater than 18%, shown in the previous section, were also fabricated with the use of MS for P2 and P3 processes. It may be challenging to apply PhLs to large-area module fabrication in practical and industrial production. Nonetheless, the results obtained in this study suggest that modification of the P3 process, for instance, the use of other patterning processes or proper passivation/termination of the MS edges (this applies to cell edges of grid-electrode structure modules), is a promising approach to further improve CIGS module efficiencies, irrespective of conventional rigid glass substrates or flexible substrates.

In conclusion, we presented the current status and perspective of lightweight and flexible CIGS solar modules. The availability and usefulness of CIGS photovoltaic devices under low illumination conditions have also been suggested. For further development, improvement of CIGS solar cell performance is essential. Approaches based on materials science and device physics, including modification of the properties of the surface and interfaces and bulk crystal quality by alloying with Ag, S, or other elements

as well as doping control of alkali metals, are expected to bring further progress in CIGS photovoltaics. In addition, the development of module fabrication processes is expected to lead to further enhancements in CIGS photovoltaic performance. It is suggested that mechanically scribed cell edges can be one of the origin of degradation in CIGS photovoltaic devices, and thus, there is room for further improvement in the device fabrication process as well as thin-film bulk material and interfacial properties.

Methods

Sample preparation

CIGS films (2 mm thick) were grown on Mo (1 mm thick)-coated substrates by a three-stage coevaporation process[31], where $(In,Ga)_2Se_3$ precursor films were prepared during the first stage using elemental In, Ga, and Se fluxes evaporated with Knudsen cells at a substrate temperature (T_S) of 350 °C. Elemental Cu and Se fluxes were supplied during the second stage at T_S of 540−550 °C, and in the third stage, elemental In, Ga, and Se were supplied using fluxes identical to those employed in the first stage at T_S of 540−550 °C. Sputtered-SLG-coated (75 nm thick) flexible zirconia ceramic sheets[32] and rigid SLG substrates were used for minimodule and small-area cell fabrication, respectively. Na- and K-, or Rb-PDT were performed using NaF and KF, or RbF evaporated by Knudsen cells in the CIGS growth chamber. NaF and KF, or RbF were supplied after CIGS film growth with Se supply at T_S of 350 °C for 10 min. The CIGS film growth chamber used in this study was designed to deposit uniform films over an area of 100 × 100 mm^2; thus, nine 30 × 30 mm^2 samples could be grown under nominally identical conditions in a single growth run. The GGI ratio used in this study was approximately 0.3, although the value used for minimodule #1 and small-area cells were slightly higher than that used for minimodule #2. After CIGS film growth, a CdS buffer layer was deposited by chemical bath deposition using an aqueous solution comprising $CdSO_4$, NH_2CSNH_2, and ammonia solutions, and water at 80 °C. The thickness of the CdS layer used for minimodule #1 was approximately 30 nm, whereas the thickness used for minimodule #2 and small-area cells was 50−60 nm. i-ZnO and ZnO:Al layers of approximately 50 and 300 nm, respectively, were deposited via sputtering, and an Ni/Al grid electrode was formed via electron-beam evaporation for solar cell fabrication. For minimodule fabrication, P1 was performed by laser scribing prior to CIGS film growth, whereas the P2 and P3 processes were performed using MS. For small-area cell fabrication, cell separation was performed using MS or PhL for CIGS devices grown in identical growth badges. The PhL process was performed using AZ5200NJ as a photoresist and a pre-baking process at 90 °C for 1 min before light exposure. After development, the CIGS devices were rinsed with pure water and post-baking was performed at 115 °C for 3 min. Finally, the CdS and ZnO layers on the CIGS surface were removed with HCl solution, followed by rinsing with acetone to remove the photoresist, which was successively rinsed with pure water and dried with N_2 gas blow. The MS process was, on the other hand,

simply performed with a metal cutter. P2 and P3 processes and small-area cell separation were performed using the same MS apparatus.

Measurements of solar minimodule and cell properties

The CIGS minimodule performance was independently measured at AIST and JET. In-house measurements of small-area cell parameters were performed with a direction from J_{SC} to V_{OC} at 25 °C under 100 mW/cm^2 (1 sun, AM 1.5 G) illumination and dark conditions. The light intensity was adjusted using ND filters for irradiance dependence measurements. An MgF$_2$ ARC was used for minimodules #1 and #2, and for small-area cells used for irradiance dependence studies (Fig. 5), whereas no ARC was used for RbF-PDT, MS, and PhL comparative studies (Fig. 4). The diode parameters of small-area cells were calculated from light and dark $J-V$ data of the best photovoltaic efficiency solar cells in each device type (w/ or w/o RbF-PDT, and MS or PhL) using the single diode model.

SEM and EBIC measurements

SEM and EBIC measurements were performed using a HITACHI S4800 instrument with acceleration voltages of 5 and 15 kV for SEM and EBIC measurements, respectively.

Declarations

DATA AVAILABILITY

The data that support the findings of this study are available from the corresponding author upon reasonable request.

AUTHOR CONTRIBUTIONS

S.I. conceived the idea and designed the research and experiments. S.I. prepared the CIGS solar cells and minimodules with technical support from coworkers listed in the Acknowledgements section, and measured and analyzed the device properties, including the calculation of diode parameters, $J-V$, EQE, SEM, and EBIC measurements. All authors have contributed to the scientific discussion. S.I. wrote the paper. All authors revised and approved the final version of the manuscript.

COMPETING INTERESTS

The authors declare no competing interests.

ADDITIONAL INFORMATION

Supplementary Information The online version contains supplementary material available at https://doi.org/xxxxxxxxxxxxxxxxxxxxx.

Correspondence and requests for materials should be addressed to Shogo Ishizuka.

Reprints and permission information is available at http://www.nature.com/reprints

Publisher's note Springer Nature remains neutral with regard to jurisdictional claims in published maps and institutional affiliations.

References

1. Powalla, M., Paetel, S., Ahlswede, E., Wuerz, R., Wessendorf, C. D. & Friedlmeier, T. M. Thin-film solar cells exceeding 22% solar cell efficiency: an overview on CdTe-, Cu(In,Ga)Se$_2$-, and perovskite-based materials. Appl. Phys. Rev. **5**, 041602 (2018).

2. de Wild-Scholten, M. J. (Mariska) Energy payback time and carbon footprint of commercial photovoltaic systems. *Sol. Energy Mater. Sol. Cells* **119**, 296–305, (2013).

3. Green, M. A., Dunlop, E. D. Hohl-Ebinger, J., Yoshita, M., Kopidakis, N., Bothe, K., Hinken, D., Rauer, M. & Hao, X. Solar cell efficiency tables (Version 60). Prog. Photovolt. Res. Appl. **30**, 687–701 (2022).

4. Dalibor, T. CIGSSe module efficiencies on the verge of 20%. *Presented at the European Materials Research Society 2022 Spring Meeting* (May 31, 2022) K.6.1.

5. Kato, T., Handa, A., Yagioka, T., Matsuura, T., Yamamoto, K., Higashi, S., Wu, J.-L., Kong, F. T., Hiroi, H., Yoshiyama, T., Sakai, T. & Sugimoto, H. Enhanced efficiency of Cd-free Cu(In,Ga)(Se,S)$_2$ minimodule via (Zn,Mg)O second buffer layer and alkali metal post-treatment. IEEE J. Photovolt. **7**, 1773–1780 (2017).

6. MiaSolé website. https://miasole.com/miasole-breaks-world-record-again-large-area-flexible-photovoltaic-module-with-18-64-efficiency/ (November 8, 2019).

7. Ishizuka, S. et al. Physical and chemical aspects at the interface and in the bulk of CuInSe$_2$-based thin-film photovoltaics. Phys. Chem. Chem. Phys. **24**, 1262–1285 (2022).

8. Hedström, J., Ohlsén, H., Bodegård, M., Kylner, A., Stolt, L., Hariskos, D., Ruckh, M. & Schock, H.-W. ZnO/CdS/Cu(In,Ga)Se$_2$ thin film solar cells with improved performance. *Conference Record of the 23rd IEEE Photovoltaic Specialists Conference*, Louisville, USA, 1993, pp. 364–371.

9. Contreras, M. A., Egaas, B., Dippo, P., Webb, J., Granata, J., Ramanathan, K., Asher, S., Swartzlander, A. & Noufi, R. On the role of Na and modifications to Cu(In,Ga)Se$_2$ absorber materials using thin-MF (M = Na, K, Cs) precursor layers. *Conference Record of the 26th IEEE Photovoltaic Specialists Conference*, Anaheim, USA, 1997, pp. 359–362.

10. Rudmann, D., da Cunha, A. F., Kaelin, M., Kurdesau, F., Zogg, H., Tiwari, A. N. & Bilger, G. Efficiency enhancement of Cu(In,Ga)Se$_2$ solar cells due to post-deposition Na incorporation. Appl. Phys. Lett. **84**, 1129–1131 (2004).

11. Chirilă, A., Reinhard, P., Pianezzi, F., Bloesch, P., Uhl, A. R., Fella, C., Kranz, L., Keller, D., Gretener, C., Hagendorfer, H., Jaeger, D., Erni, R., Nishiwaki, S., Buecheler, S. & Tiwari, A. N. Potassium-induced surface modification of Cu(In,Ga)Se$_2$ thin films for high-efficiency solar cells. Nat. Mater. **12**, 1107–1111 (2013).

12. Jackson, P., Wuerz, R., Hariskos, D., Lotter, E., Witte, W. & Powalla, M. Effects of heavy alkali elements in Cu(In,Ga)Se$_2$ solar cells with efficiencies up to 22.6%. Phys. Status Solidi RRL **10**, 583–586 (2016).

13. Nakamura, M., Yamaguchi, K., Kimoto, Y., Yasaki, Y., Kato, T. & Sugimoto, H. Cd-free Cu(In,Ga)(Se,S)$_2$ thin-film solar cell with record efficiency of 23.35%. IEEE J. Photovolt. **9**, 1863–1867 (2019).

14. Ishizuka, S., Taguchi, N. & Fons, P. J. Similarities and critical differences in heavy alkali-metal rubidium and cesium effects on chalcopyrite Cu(In,Ga)Se$_2$ thin-film solar cells. J. Phys. Chem. C **123**, 17757–17764 (2019).

15. Ishizuka, S. & Fons, P. J., Lithium-doping effects in Cu(In,Ga)Se$_2$ thin-film and photovoltaic properties. ACS Appl. Mater. Interfaces **12**, 25058–25065 (2020).

16. Nishinaga, J., Koid, T., Ishizuka, S., Kamikawa, Y., Takahashi, H., Iioka, M., Higuchi, H., Ueno, Y., Shibata, H. & Niki, S. Effects of long-term heat-light soaking on Cu(In,Ga)Se$_2$ solar cells with KF postdeposition treatment. Appl. Phys. Express **10**, 092301 (2017).

17. Khatri, I., Matsuura, J., Sugiyama, M. & Nakada, T. Effect of heat-bias soaking on cesium fluoride-treated CIGS thin film solar cells. Prog. Photovolt. Res. Appl. **27**, 22–29 (2019).

18. Lundberg, O., Edoff, M. & Stolt, L. The effect of Ga-grading in CIGS thin film solar cells. Thin Solid Films **480–481**, 520–525 (2005).

19. Erslev, P. T., Lee, J., Hanket, G. M., Shafarman, W. N. & Cohen, J. D. The electronic structure of Cu(In$_{1-x}$Ga$_x$)Se$_2$ alloyed with silver. Thin Solid Films **519**, 7296–7299 (2011).

20. Chen, L., Lee, J. & Shafarman, W. N. The comparison of (Ag,Cu)(In,Ga)Se$_2$ and Cu(In,Ga)Se$_2$ thin films deposited by three-stage coevaporation. IEEE J. Photovolt. **4**, 447–451 (2014).

21. Yoon, J.-H., Kim, J.-H., Kim, W. M., Park, J.-K., Baik, Y.-J., Seong, T.-Y. & Jeong, J.-H. Electrical properties of CIGS/Mo junctions as a function of MoSe$_2$ orientation and Na doping. Prog. Photovolt. Res. Appl. **22**, 90–96 (2014).

22. Yang, S.-C., Sastre, J., Krause, M., Sun, X., Hertwig, R., Ochoa, M., Tiwari, A. N. & Carron, R. Silver-promoted high-performance (Ag,Cu)(In,Ga)Se$_2$ thin-film solar cells grown at very low temperature. Sol. RRL **5**, 2100108 (2021).

23. Weiss, T. P., Ehre, F., Serrano-Escalante, V., Wang, T. & Siebentritt, S. Understanding performance limitations of Cu(In,Ga)Se$_2$ solar cells due to metastable defects – A route toward higher efficiencies. Sol. RRL **5**, 2100063 (2021).

24. Stanbery, B. J., Abou-ras, D., Yamada, A. & Mansfield L. CIGS photovoltaics: reviewing an evolving paradigm. J. Phys. D: Appl. Phys. **55**, 173001 (2022).

25. Gecys, P., Raciukaitis, G., Wehrmann, A., Zimmer, K., Braun, A. & Ragnow, S. Scribing of thin-film solar cells with picosecond and femtosecond lasers. J. Laser Micro Nanoeng. **7**, 33–37 (2012).

26. Narazaki, A. et al. Evaluation of femtosecond laser-scribed Cu(In,Ga)Se$_2$ solar cells using scanning spreading resistance microscopy. Appl. Phys. Express **11**, 032301 (2018).

27. Niki, S., Contreras, M., Repins, I., Powalla, M., Kushiya, K., Ishizuka, S. & Matsubara, K. CIGS absorbers and processes. Prog. Photovolt. Res. Appl. **18**, 453–466 (2010).

28. Ishizuka, S., Shibata, H., Nishinaga, J., Kamikawa, Y. & Fons, P. J. Effects of RbF postdeposition treatment and heat-light soaking on the metastable acceptor activation of CuInSe$_2$ thin film photovoltaic devices. Appl. Phys. Lett. **113**, 063901 (2018).

29. Ishizuka, S., Yamada, A., Fons, P. & Niki, S. Texture and morphology variations in (In,Ga)$_2$Se$_3$ and Cu(In,Ga)Se$_2$ thin films grown with various Se source conditions. Prog. Photovolt. Res. Appl. **21**, 544–553 (2013).

30. Virtuani, A., Lotter, E. & Powalla, M. Performance of Cu(In,Ga)Se$_2$ solar cells under low irradiance. Thin Solid Films **431–432**, 443–447 (2003).

31. Gabor, A. M., Tuttle, J. R., Albin, D. S., Contreras, M. A., Noufi, R. & Hermann, A. M. High-efficiency CuIn$_x$Ga$_{1-x}$Se$_2$ solar cells made from (In$_x$Ga$_{1-x}$)$_2$Se$_3$ precursor films. Appl. Phys. Lett. **65**, 198–200 (1994).

32. Ishizuka, S., Yamada, A., Fons, P. & Niki, S. Flexible Cu(In,Ga)Se$_2$ solar cells fabricated using alkali-silicate glass thin layers as an alkali source material. J. Renew. Sustain. Energy **1**, 013102 (2008).

Tables

Table 1. Performance of lightweight and flexible monolithically interconnected CIGS minimodules

Minimodule	PDT	Efficiency (%)	V_{OC} (V)	I_{SC} (mA)	FF (%)	Area (cm^2)	No. of cells	Test center
#1[7]	RbF	18.64	12.70	138.5	72.0	68.0 (d.a.)	17	AIST
#2	NaF + KF	18.5	12.13	136.8	75.8	67.95 (d.a.)	17	JET

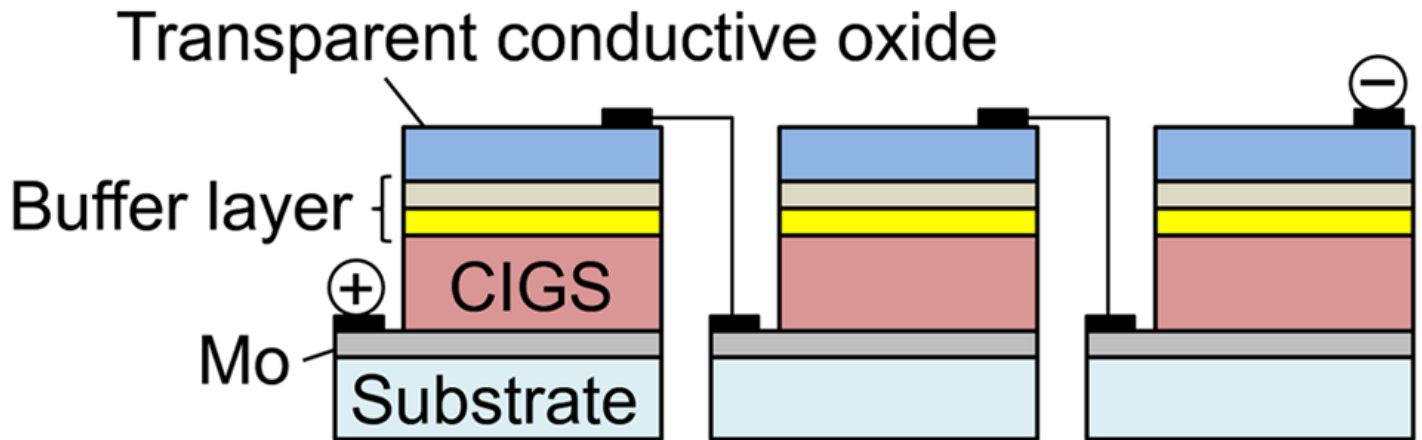I_{SC}: Short circuit current. d.a.: designated area.

Table 2. Diode parameters obtained for MS- and PhL-processed CIGS solar cells

Scribing	RbF-PDT	R_{sh} (W cm^2)	R_s (W cm^2)	A	J_0 (mA/cm^2)
Dark					
MS	No	1289	0.38	1.46	1.00E-07
MS	Yes	1118	0.46	1.43	4.70E-08
PhL	No	Inf.	0.38	1.40	5.00E-08
PhL	Yes	Inf.	0.25	1.43	3.80E-08
Light					
MS	No	803	0.06	1.71	3.30E-06
MS	Yes	715	0.27	1.54	2.70E-07
PhL	No	5393	0.12	1.66	2.00E-06
PhL	Yes	7102	0.22	1.52	1.90E-07

Inf.: Nominally infinite.

Figures

a Grid electrode structure

Transparent conductive oxide

Buffer layer {

CIGS

Mo

Substrate

⊖

⊕

b Monolithically interconnected structure

P3

P2

P1

⊕

⊖

Substrate
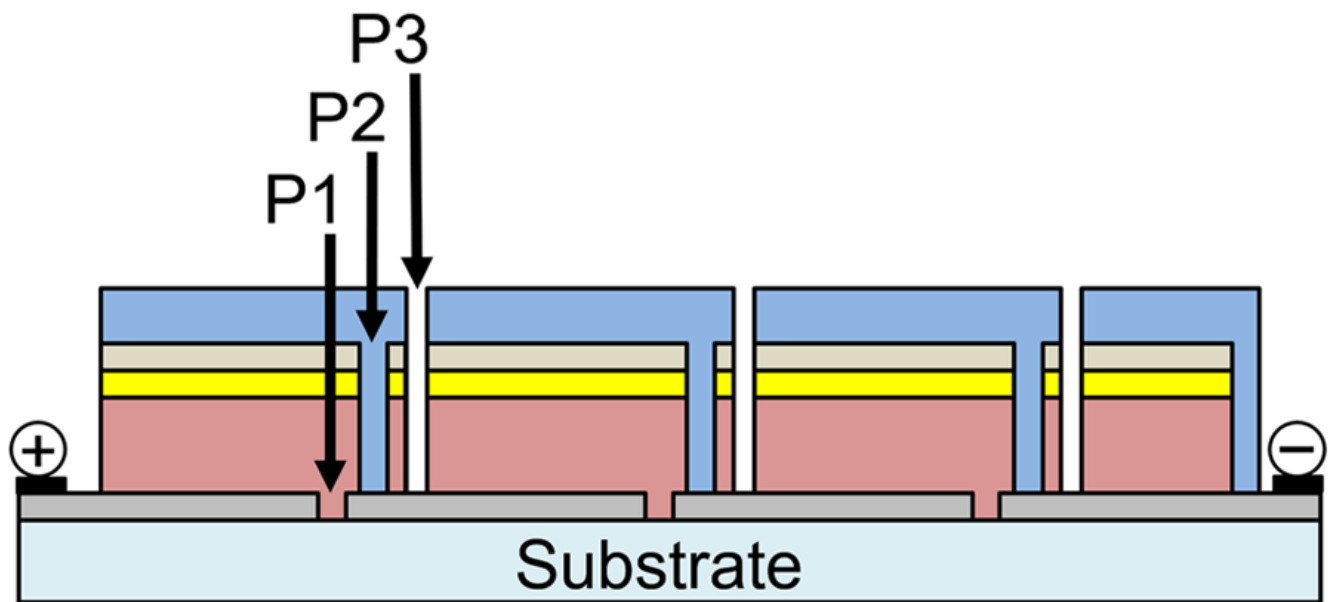
Figure 1

Schematic of CIGS solar module structure. a Grid electrode module. **b** monolithically interconnected module.
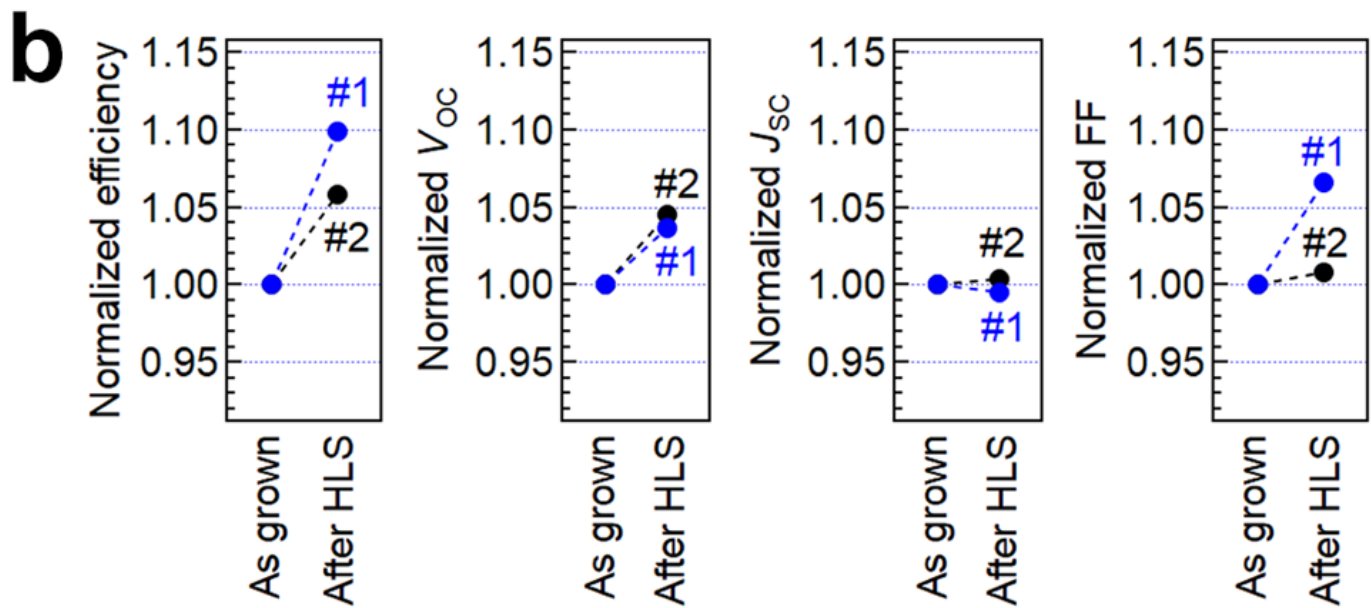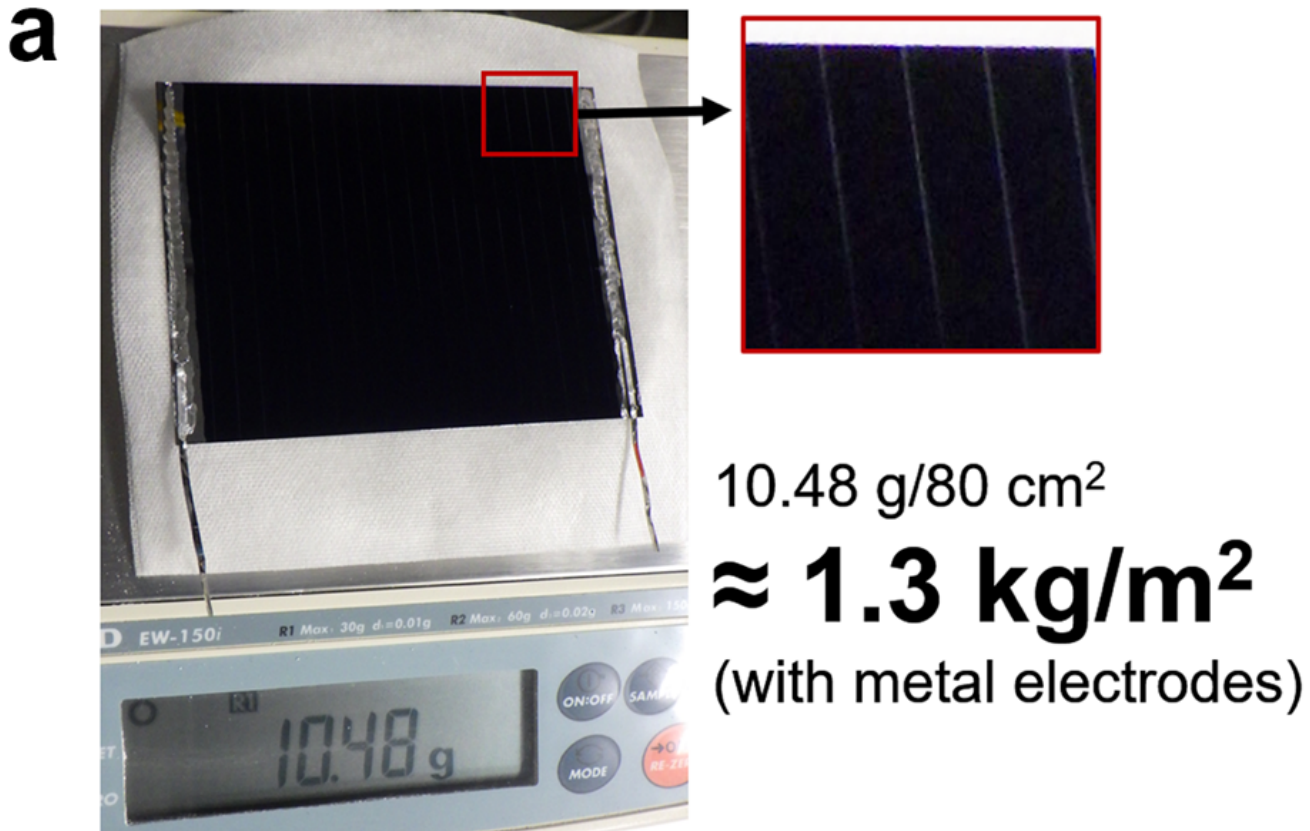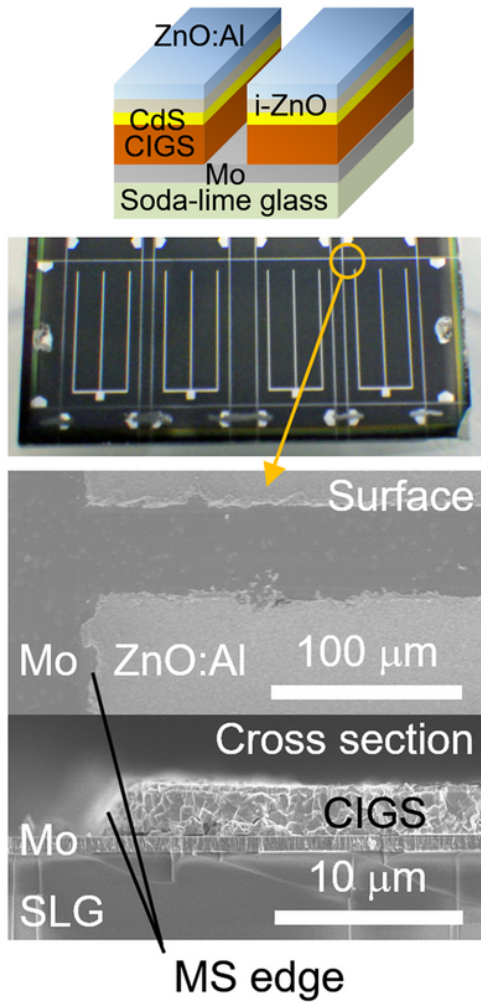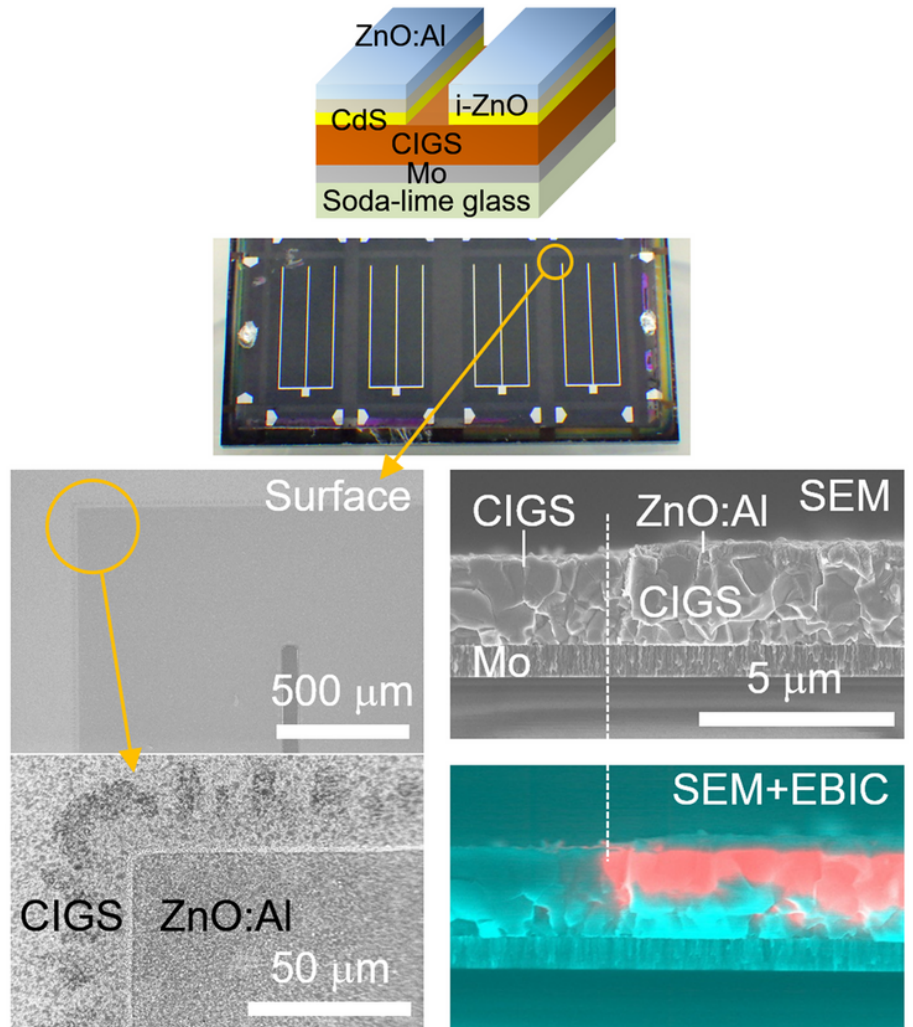
Figure 2

CIGS solar minimodule properties. **a** Photograph of CIGS solar minimodule #1. **b** Variations in CIGS minimodule properties with HLS treatments.

Figure 3

Scribing edges formed with MS and PhL. **a** Schematic of MS-processed edges and a corresponding photograph and scanning electron microscopy (SEM) images. **b** Schematic of PhL-processed edges and a corresponding photograph and SEM and EBIC images.
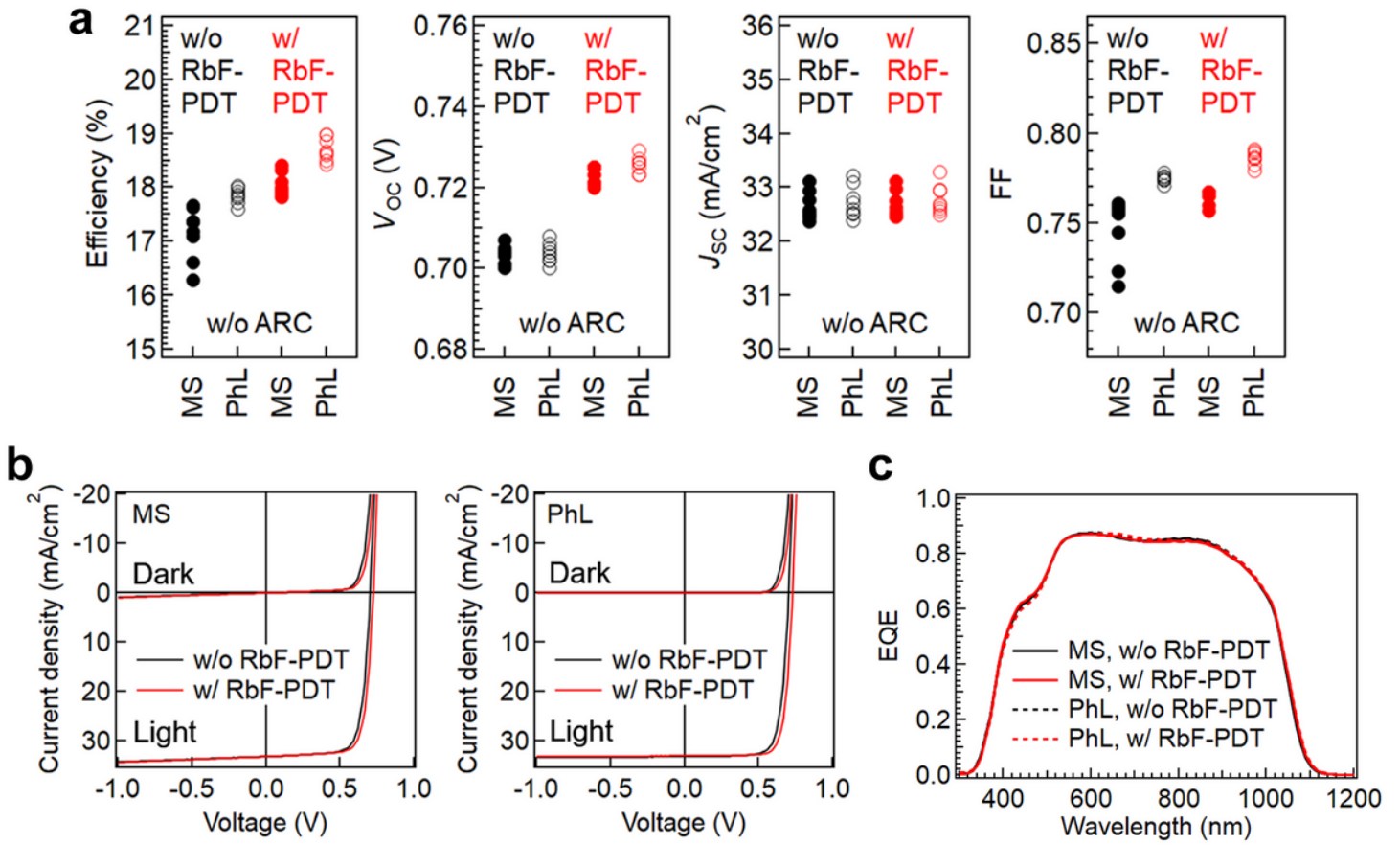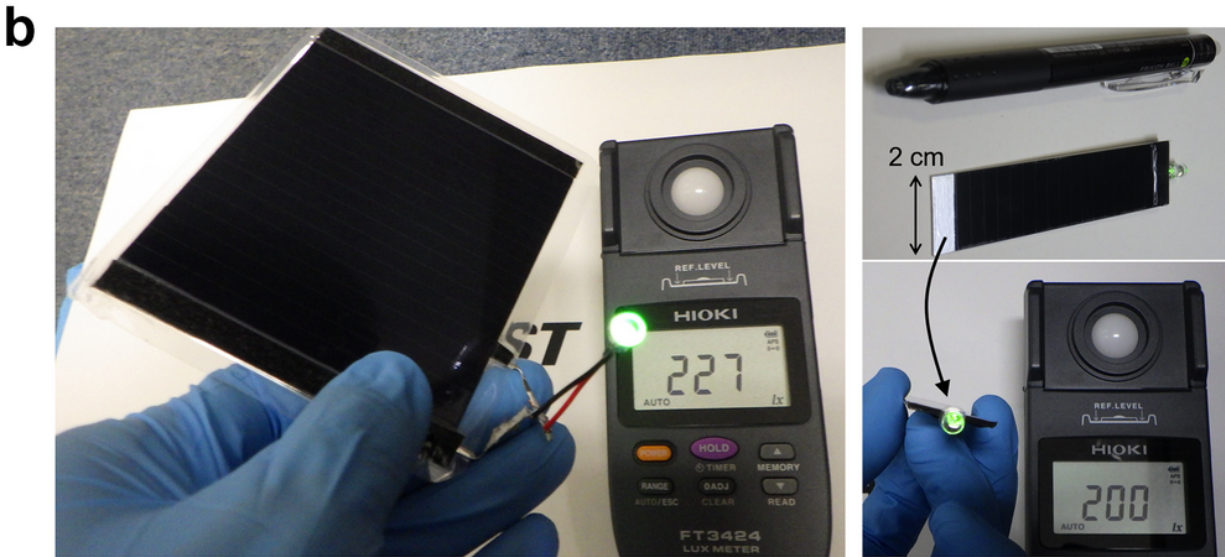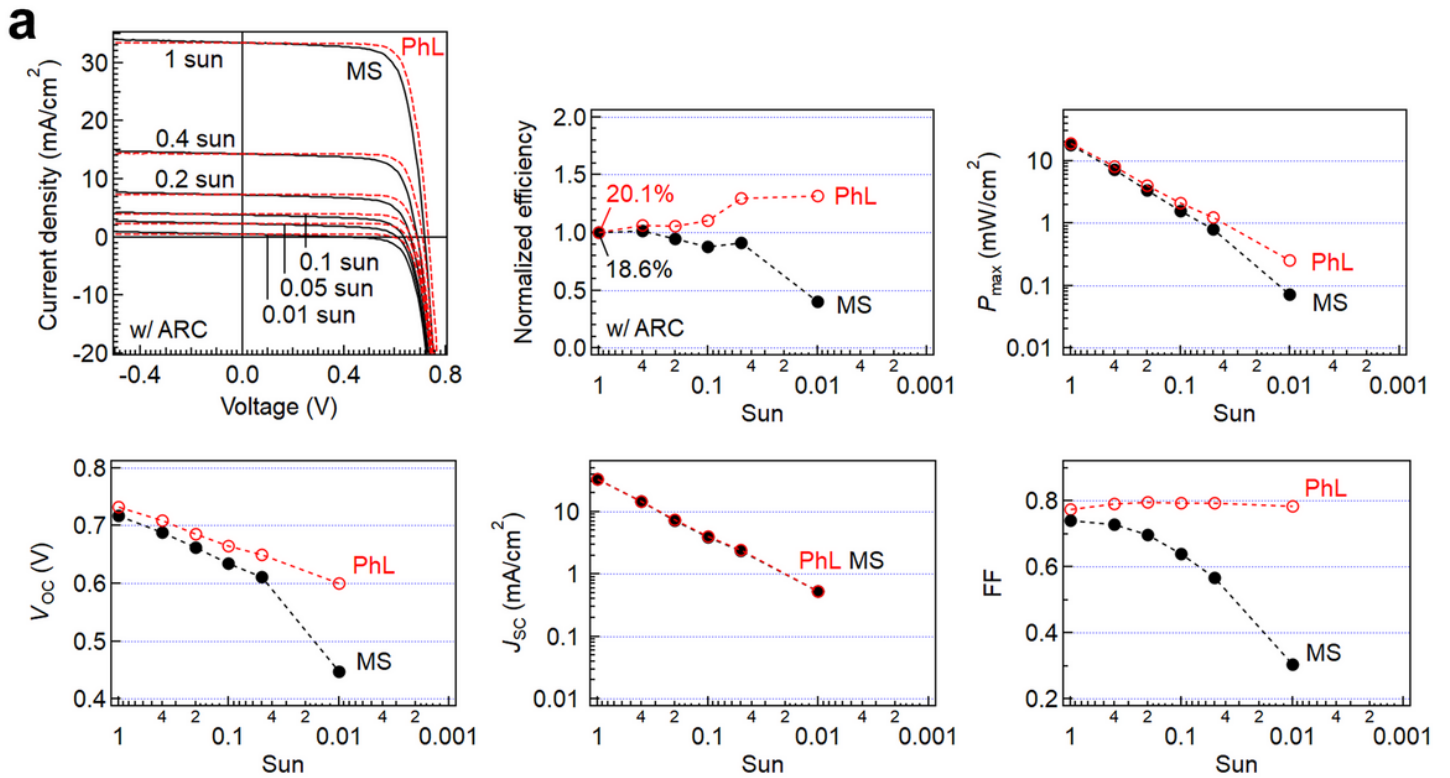
Figure 4

Comparison of MS- and PhL-processed solar cell properties. a Variations in solar cell parameters. **b** $J{-}V$ and **c** EQE curves obtained from corresponding cells.

Figure 5

Light intensity dependence of CIGS solar cells. **a** *J−V* curves and corresponding solar cell parameter variations observed for 0.5 cm^2 size CIGS cells. **b** Photographs of practical usage of lightweight and flexible CIGS minimodules lighting a green LED under approximately 200 lx illumination.